Mechanics-Based Design of Underactuated Robotic Walking Gaits: Initial Experimental Realization

Matthew J. Powell, Wen-Loong Ma, Eric R. Ambrose and Aaron D. Ames

***Abstract*— This paper presents two strategies for designing underactuated, planar robotic walking gaits and for realizing them experimentally. The methods draw upon insights gained from the authors' recent work which leverages properties of the mechanics of the robot to design a controller that stabilizes walking by regulating the transfer of angular momentum about one support pivot to the next. One proposed gait design strategy is to simulate a closed-loop hybrid model of the robot under the action of the mechanics-based controller to produce an implicit periodic orbit for each set of controller parameters. The second design strategy modifies traditional usage of nonlinear optimization to produce parameterized outputs corresponding to a stable Hybrid Zero Dynamics. The novel approach is to reformulate the HZD stability constraint using the mechanics of the system and to propose an alternative to the periodic HZD orbit existence constraint through the use of an angular momentum variant of the Linear Inverted Pendulum. The two methods are used to design gaits that are implemented in experiments with the AMBER-3M robot.**

I. INTRODUCTION

To realize the full potential of humanoid robots as valuable tools for the general public, contemporary research is aimed at developing controllers that achieve unassisted walking in unstructured environments. It is important to note, however, that the controller design process often starts with simpler, planar analysis and experiments. Many of the recent experimental robot locomotion controller implementations, such as [6], [13], [14], [19], [23], can be traced to simpler, planar origins. Following this workflow, the goal of this paper is to present strategies for designing walking gaits – using the principles described in the authors' recently proposed approach for achieving theoretical 3D walking [20] – for the purpose of initial experimental implementation and testing on the planar AMBER-3M robot, shown in Fig. 1.

The notion of a walking gait considered in this paper is intimately connected with the choice of (hybrid) robot model [10]; in this context, robotic walking gaits correspond to periodic solutions in the hybrid system. This allows for verification of the stability of walking gaits to be computed through rigorous stability analysis, namely the method of Poincaré [11]. Extensions of this analysis have shown that through proper design of continuous-time control, stability of a closed-loop walking gait can be related to the stability of a subset of the system's coordinates termed the Hybrid Zero Dynamics (HZD) [18], [27]. The HZD gait design framework

This research is supported by the NSF grant CPS-1239055.

Matthew J. Powell, Wen-Loong Ma, Eric R. Ambrose and Aaron D. Ames are with the George W. Woodruff School of Mechanical Engineering, Georgia Institute of Technology, Atlanta, GA 30308. {mpowell35,wenlongma,eambrose,ames}@gatech.edu

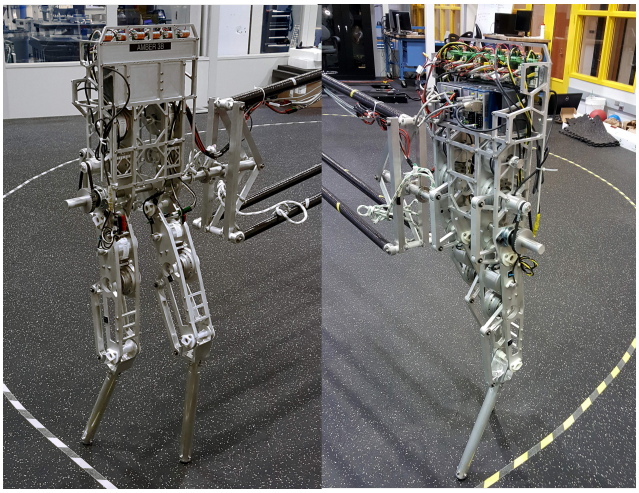

Fig. 1. AMBER-3M: the modular bipedal robot custom-built by AMBER Lab. It has multiple leg configurations to test different walking types—in this case, the point-foot setup is considered.

provides a set of nonlinear constraints on the gait parameters which – if satisfied – imply the gait is locally exponentially stable. The original HZD framework solved these constraints through nonlinear optimization, and indeed, most hybrid-system gait generation methods have used optimization to-date. However, new methods [22] and [16] are capable of producing periodic orbits without optimization.

It has been noted that one of the zero dynamics coordinates in underactuated walking is the angular momentum about the stance pivot [4]. This observation motivated the authors' mechanics-based approach that is built around the goal of controlling the transfer of angular momentum from one support pivot to the next [20]. The present paper proposes two strategies for generating gaits through the mechanics-based control principles for the purpose of experimental validation. The first is to generate gaits implicitly – i.e. without optimization – by simulating the closed-loop hybrid system under mechanics-based control until it converges to an orbit. The second gait design strategy uses the connection between the zero dynamics and the mechanics of underactuated walking to modify Hybrid Zero Dynamics based nonlinear gait optimization methods. Both design strategies ultimately produce parameterized functions encoding walking gaits; these functions are used in conjunction with inverse kinematics to implement the gait in position-control experiments with the AMBER-3M robot.

The proposed gait design philosophy is to expose the general mechanics of underactuated walking and then build controllers to manipulate these mechanics. This approach

is just one of many usages of Classical Mechanics [7], which has played a large role in the development of several humanoid walking control principles and strategies to-date. The Zero Moment Point concept uses the relationship between the center of mass acceleration and the reaction forces acting on footed robots to establish foot-rotation-stability criteria [26]. Assumptions on the mechanics of the system can be used to reduce the nonlinear rigid-body dynamics into more tractable systems such as the Linear Inverted Pendulum [15], which has seen tremendous success in walking control design [21], [25]. And adding angular momentum feedback to HZD-based virtual constraint optimization results in increased robustness to perturbations in the walking surface [9]. The current paper intends to add to the existing walking mechanics literature by illuminating useful properties of the *hybrid mechanics of underactuated walking*.

II. Planar Underactuated Walking

The robot of interest in this paper is a underactuated biped: it has five degrees of freedom but only four actuators located at the robot's knee and hip joints. The fifth degree of freedom – located at the support 'ankle' – is not actuated. This section begins with a brief overview of the hybrid system [10] used to model the robot.

A. Hybrid System Model and Walking Gaits

Let $\theta \in \mathbb{R}^5$ denote the robot's joint angles, let $x = (\theta, \dot{\theta})$ denote the robot's states and let $u \in \mathbb{R}^4$ denote the torques applied by the robot's actuators. Under a choice of feedback control $u = u(x)$, the behavior of the robot is modeled as a closed-loop hybrid dynamical system with both continuous-time, rigid-body dynamics $\dot{x} = f(x)$ and discrete changes in state $x^+ = \Delta(x^-)$ that occur when the robot's swing foot strikes the ground. At these impacts, Δ models the jump from the state just-prior to impact, x^-, to the state just-after impact (and leg swap) x^+. See [10] for details on f, Δ, options for $u(x)$ and construction of the hybrid model.

The evolution of the states in this hybrid system can be compactly represented using Poincaré map techniques. In particular, the state of the robot, $x^-[k+1]$, just-prior to impact in the end of step $k+1$, is given by

$$x^-[k+1] = \Delta\left(x^-[k]\right) + \int_0^{T[k+1]} f(x(t))dt \qquad (1)$$

where $T[k+1] = T(\Delta(x^-[k]))$. In this paper, walking gaits correspond to periodic solutions of the hybrid system which further correspond to fixed points of (1); i.e. $x^-[k+1] = x^-[k] = x^*$, for $k = 1, 2, \ldots$ Numeric Poincaré analysis is often used to verify the local stability of a walking gait [11].

As the particular robot considered is underactuated, creating stable walking gaits can be challenging: underactuation corresponds to nonlinear dynamics that are not affected by the robot's motors and thus not locally controllable. A key observation, however, is that one of the components of the underactuated dynamics corresponds to the rate of change of angular momentum about the robot's support pivot. This fact motivates the proposed strategies for designing walking gaits which leverage properties of the angular momentum about the stance pivot in order to uncover new insights into the uncontrolled dynamics in underactuated walking.

B. The Mechanics of Underactuated Walking

The (mass-normalized) angular momentum, L_y, about the support pivot along the continuous flow can be expressed as

$$L_y = z_c\dot{x}_c - x_c\dot{z}_c + \frac{H_c}{M} \qquad (2)$$

where $x_c = x_c(\theta)$ and $z_c = z_c(\theta)$ denote the horizontal and vertical positions of the center of mass relative to the stance pivot, $H_c = H_c(\theta, \dot{\theta})$ is the centroidal angular momentum, and M is the total mass of the robot. In the model of interest, the support leg pivots freely about an ideal pin-joint (the support ankle). Note that the only external moment acting on this pivot is due to gravity, thus by Newton's second law

$$\dot{L}_y = gx_c \qquad (3)$$

where g is the acceleration due to gravity. Although $\dot{L}_y$, when computed by taking the derivative of (2), does contain the joint accelerations $\ddot{\theta}$, which are themselves functions of the choice of feedback control u, Newtonian mechanics indicates that $\dot{L}_y$ is actually independent of the choice of u (for this particular point-foot robot). Specifically, the r.h.s. of (3) is only a function of the joint angles θ through $x_c = x_c(\theta)$. This implies that (2) and (3) are a part of *all underactuated walking behaviors*, and that L_y is *not locally controllable*.

In the context of the hybrid model of walking, the discrete-time momentum mechanics also plays a large role. The transfer of (mass-normalized) angular momentum from one support pivot to the next – i.e. the discrete-time momentum mechanics – on flat ground can be expressed as

$$L_y^+[k+1] = L_y^-[k] + x_n^-[k]\dot{z}_c^-[k], \qquad (4)$$

where $x_n = x_n(\theta)$ is the horizontal nonstance foot position relative to the support pivot. As noted in [20], while the (local) continuous-time evolution of L_y is uncontrollable, the hybrid evolution of L_y can be controlled through control of x_n and $\dot{z}_c$ using (4) and the following qualitative characterization of the continuous-time angular momentum.

C. Angular Momentum Variant of the LIP

The angular momentum variant of the Linear Inverted Pendulum (LIP) [15] is given by the system

$$L_y = z_0\dot{x}_c, \qquad (5)$$

$$\dot{L}_y = gx_c, \qquad (6)$$

where z_0 is a constant height of the center of mass. The phase space of the angular momentum LIP – shown in Fig. 2 – provides a qualitative characterization of the evolution of L_y and x_c in the nonlinear system for $z_c\dot{x}_c >> -x_c\dot{z}_c + H_c/M$. Note that the asymptotes $L_y = \pm\sqrt{gz_0}x_c$ divide the phase space into four quadrants, and that the top quadrant corresponds to forward walking. This characterization suggests that in order to ensure forward walking in the nonlinear hybrid system model (1), the post-impact x_c^+ and L_y^+ should always take values in the top quadrant of the LIP phase space.

III. Implict Gait Design via Mechanics-Based Control

The properties of the hybrid mechanics discussed in the previous section were used to motivate the Mechanics-Based Controller (MBC) proposed in [20]; this section discusses how to use MBC to design walking gaits for the purpose of experimental implementation. The benefit to this approach is that different gaits can be obtained by changing the five controller parameters. However, as the method does not enforce hybrid output invariance, the gaits are not known explicitly. Therefore, a gait is obtained implicitly by simulating the closed-loop hybrid system until it converges to an orbit.

A. Mechanics-Based Control

The mechanics-based controller in [20] is ultimately manifested in the construction of desired outputs for the robot's nonstance foot position, x_n and z_n, vertical center of mass, z_c, and torso orientation, ϕ_t. These outputs take the form

$$y(\theta,\dot{\theta}) = \begin{bmatrix} x_n(\theta) \\ z_n(\theta) \\ z_c(\theta) \\ \phi_t(\theta) \end{bmatrix} - \begin{bmatrix} x_n^d(x_c,\mathbf{k_x}(x_c,L_y)) \\ z_n^d(x_c,\mathbf{k_z}(x_c,L_y)) \\ z_c^d(x_c,\mathbf{k_c}(x_c,L_y)) \\ 0 \end{bmatrix}, \quad (7)$$

where $x_c = x_c(\theta)$ and $L_y = L_y(\theta,\dot{\theta})$. Note that x_n^d, z_n^d and z_c^d can be simple functions of x_c. The key to MBC is the design of the coefficients of these functions, i.e. the design of $\mathbf{k_x}$, $\mathbf{k_z}$, $\mathbf{k_c}$ which dynamically update as x_c and L_y evolve.

The coefficients encode the goal of simultaneously swinging the leg forward while also ensuring that the uncontrolled coordinates – the angular momentum and the horizontal center of mass – are regulated in the hybrid evolution of the system. As noted in Section II-B, the post-impact angular momentum can be manipulated by controlling the pre-impact step length and vertical COM velocity according to the discrete mechanics (4). This together with the fact that $x_c^+ = x_c^- - x_n^-$, provides a set of "boundary conditions" on the desired trajectories when the system reaches (x_c^-, L_y^-)

$$x_n^d(x_c^-,\mathbf{k_x}) = x_c^- - x_c^*, \quad (8)$$

$$\dot{z_c}^d(x_c^-,\mathbf{k_c}) = \frac{L_y^* - L_y^-}{x_c^- - x_c^*}, \quad (9)$$

$$z_n^d(x_c^-,\mathbf{k_z}) = 0, \quad (10)$$

for a given desired post-impact x_c^* and L_y^*.

The solution of the angular momentum LIP dynamics (5)–(6) is used to compute a forward horizon estimate $\hat{x}_c^-(\theta,\dot{\theta})$ of what x_c^- will be when L_y^- reaches a given L_y^{d-}

$$\hat{x}_c^-(\theta,\dot{\theta}) = \sqrt{\frac{\left(L_y^{d-}\right)^2}{gz_0} - \frac{L_y(\theta,\dot{\theta})^2}{gz_0} + x_c^2(\theta)}. \quad (11)$$

This value is estimated continuously throughout the step, and converges to the value of $x_c(\theta)$ in the nonlinear system as $L_y(\theta,\dot{\theta})$ approaches L_y^{d-}. This estimate (11) is substituted for x_c^- in the boundary conditions (8)–(10) and used, in conjunction with additional boundary constraints, to dynamically calculate the coefficients $\mathbf{k_x}$, $\mathbf{k_z}$, and $\mathbf{k_c}$. Using control to stabilize outputs of this form results in stable periodic walking in simulation for a range of controller parameters.

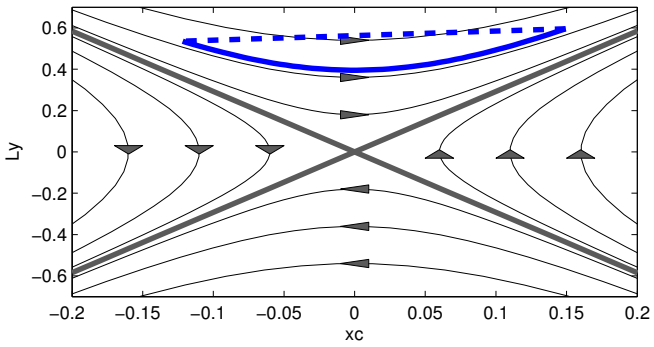

Fig. 2. (Gray) The phase space of the angular momentum variant of the Linear Inverted Pendulum, described by the system (5)–(6), with $z_0 = 0.87\text{m}$. (Blue) Simulation of the nonlinear hybrid walking model (1) of AMBER-3M under the control described in Section III. The solid blue line is the continuous-time evolution of the x_c and L_y coordinates, described by (2) and (3), and the dashed line indicates the discrete mechanics (4).

B. Implicit Gait Design Process

Given a choice of mechanics-based controller outputs (7), a gait can be created by first choosing controller parameters, including x_c^*, L_y^*, then solving an inverse kinematics problem

$$(\theta(0),\dot{\theta}(0)) = (\theta,\dot{\theta}) \quad s.t. \quad (12)$$
$$y(\theta,\dot{\theta}) = \dot{y}(\theta,\dot{\theta}) = 0,\ x_c(\theta) = x_c^*,\ L(\theta,\dot{\theta}) = L_y^*.$$

The gait is then obtained by simulating the closed loop hybrid system (1), starting from $\theta(0)$ and $\dot{\theta}(0)$, under a controller that drives $y \to 0$, e.g. Feedback Linearization [24], until the hybrid system converges to a periodic orbit. If the robot falls over, the process is repeated for a new x_c^*, L_y^* that is further in the interior of the upper quadrant of the LIP phase space.

C. Desired Functions and Adjustments for Experimental Use

For this work, the following desired basis functions were chosen over the original set of functions put forth in [20]

$$x_n^d(x_c,\mathbf{k_x}(x_c,L_y)) = k_{x,1}x_c^3 + k_{x,2}x_c^2 + k_{x,3}x_c + k_{x,4},$$
$$z_n^d(x_c,\mathbf{k_z}(x_c,L_y)) = z_n^{max}\sin(k_{z,1}x_c + k_{z,2}),$$
$$z_c^d(x_c,\mathbf{k_c}(x_c,L_y)) = z_0 + \delta_z\sin(k_{c,1}x_c + k_{c,2}).$$

Adding sinusoidal oscillation to the (constant) height of the center of mass results in reduced joint-velocities. Note that this choice of z_c^d does not allow for specification of both L_y^* and L_y^{d-}, however, picking L_y^{d-} allows for the resulting L_y^* to be tuned through (9) by manipulating δ_z.

These functions are used in the experimental deployment of the gait, however, the angular momentum computed on the measured encoder velocities is currently unusable as a feedback signal. Thus in the experimental implementation, presented in Section V, the dynamic update (11) is disabled and a fixed value of x_c^- – obtained from simulation – is used in boundary conditions (8)–(10), resulting in a "feedforward" gait. Future work will include angular momentum feedback, and thus increase the robustness of the experimental walking.

IV. Optimized HZD Gait Design with Mechanics-Based Constraints

This section describes an alternative method of employing the insights gained from the mechanics of underactuated walking; here they are used to modify constraints in traditional optimization-based Hybrid Zero Dynamics gait design. The aim of the this proposed approach is to use optimization to produce hybrid-invariant, energy-efficient gaits while also exposing the mechanical structure of the constraints.

A. Traditional Hybrid Zero Dynamics Optimization

The traditional hybrid zero dynamics optimization approach to designing walking gaits ultimately results in the specification of outputs of the form [3]

$$y(\theta) = y^a(\theta) - y^d(\tau(\theta), \alpha) \tag{13}$$

where for the model considered, y^d is a set of four basis functions that encode the desired behavior for the corresponding actual quantities y^a, and $\tau(\theta)$ is a monotonically increasing function. Parameters α^* of the desired functions, and a fixed point $(\theta(\alpha^*), \dot{\theta}(\alpha^*))$ corresponding to a stable walking gait are obtained by solving a nonlinear optimization of the form

$$\alpha^* = \underset{\alpha \in \mathbb{R}^{n_\alpha}}{\operatorname{argmin}} \; J(\alpha) \tag{14}$$

$$\text{s.t.} \quad \Delta(S \cap Z(\alpha)) \subset Z(\alpha) \tag{15}$$

$$0 < \delta^2_{\text{zero}}(\alpha) < 1 \tag{16}$$

$$\frac{\delta^2_{\text{zero}}(\alpha)}{1 - \delta^2_{\text{zero}}(\alpha)} V_{\text{zero}}(\alpha) + K(\alpha) < 0 \tag{17}$$

$$C_p(\alpha) < 0. \tag{18}$$

In this paper $J(\alpha)$ is the mechanical cost of transport listed in [5], and $C_p(\alpha)$ are physical constraints, e.g. actuator limits. See [27] for definitions of Δ, S, Z, δ_{zero}, V, and K.

The constraint $\Delta(S \cap Z(\alpha)) \subset Z(\alpha)$ ensures that the zero dynamics surface, $Z(\alpha)$, associated with the outputs y in (13) is invariant through intersection with the guard S and application of the reset map Δ. This *hybrid invariance* constraint reduces analysis of the stability of the walking gait to analysis of the stability of a two-dimensional hybrid system, with coordinates (ξ_1, ξ_2), termed the Hybrid Zero Dynamics. The Poincaré map for the Hybrid Zero Dynamics, with change of coordinates $\zeta_2 = \frac{1}{2}\xi_2^2$, is given in (53) of [27]

$$\zeta_2^-[k+1] = \delta^2_{\text{zero}}(\alpha)\zeta_2^-[k] - V_{\text{zero}}(\theta^-(\alpha)) \tag{19}$$

The constraint $\frac{\delta^2_{\text{zero}}(\alpha)}{1-\delta^2_{\text{zero}}(\alpha)} V_{\text{zero}}(\alpha) + K(\alpha) < 0$ ensures existence of periodic orbits in the HZD. The constraint $0 < \delta^2_{\text{zero}}(\alpha) < 1$ implies stability of an HZD orbit, which further implies stability of the walking gait [27], [18].

A key observation connecting Hybrid Zero Dynamics and the mechanics of walking is that the coordinate ξ_2 is the angular momentum about the stance pivot, i.e. $\xi_2 \equiv L_y$ [4]. Thus, an alternative interpretation of Theorems in [11], [27] and [18] is that the stability of a walking gait can be established by creating a stable Poincaré map for the angular momentum. This interpretation motivates the following reformulation of (19) and (16) using the properties of the mechanics discussed in Section II-B.

B. Mechanics Structure of the HZD Stability Constraint

As $\xi_2 \equiv L_y$, the mechanics of walking, namely (3) and (4), can be used to construct a Poincaré map analogous to (19) for the angular momentum

$$L_y^-[k+1] = L_y^-[k] + x_n^-[k]\dot{z}_c^-[k] + \int_0^{T[k]} g x_c(t) dt. \tag{20}$$

Inverse kinematics on $Z(\alpha)$ can be used to further expose the structure of (20). In particular, the angles and velocities of the robot at impact on $Z(\alpha)$ are functions of α and L_y^-

$$\theta^-(\alpha) = \theta \quad \text{s.t.} \begin{bmatrix} y(\theta) \\ z_n(\theta) \end{bmatrix} = \begin{bmatrix} \mathbf{0} \\ 0 \end{bmatrix} \tag{21}$$

$$\dot{\theta}^-(\alpha, L_y^-) = \dot{\theta} \quad \text{s.t.} \begin{bmatrix} \frac{\partial y}{\partial \theta}(\theta^-(\alpha)) \\ -\frac{D_{1,:}(\theta^-(\alpha))}{M} \end{bmatrix}^{-1} \begin{bmatrix} \mathbf{0} \\ 1 \end{bmatrix} L_y^- \tag{22}$$

where $D_{1,:}(\theta)$ is the row of the inertia matrix corresponding to the angular momentum of the robot about the stance pivot, i.e. here $L_y = -(1/M)D_{1:}(\theta)\dot{\theta}$ [27]. Defining

$$w(\alpha) = x_n(\theta^-(\alpha))\frac{\partial z_c}{\partial \theta}(\theta^-(\alpha)) \begin{bmatrix} \frac{\partial y}{\partial \theta}(\theta^-(\alpha)) \\ -\frac{D_{1,:}(\theta^-(\alpha))}{M} \end{bmatrix}^{-1} \begin{bmatrix} \mathbf{0} \\ 1 \end{bmatrix}$$

and substituting into (20) yields a form analogous to (19)

$$L_y^-[k+1] = (1 + w(\alpha))L_y^-[k] + \int_0^{T[k]} g x_c(t) dt. \tag{23}$$

Using a change of variables $\zeta_2 := \frac{1}{2}(L_y)^2$ presented in (45)-(46) of [27], it can be shown that on $Z(\alpha)$, the integral term in (23) is independent of L_y and thus the momentum Poincaré map is exponentially stable if

$$-1 < w(\alpha) < 0. \tag{24}$$

This constraint will be used to replace (16) in (14).

C. Mechanics-Based Forward Walking Constraint

As the angular momentum is uncontrollable in continuous-time, proper gait design must ensure that the post-impact L_y along the gait is sufficiently high for the robot to complete the next step. This is reflected in the HZD constraint (17). For an alternative to (17), we propose to enforce that the initial x_c and L_y are sufficiently within the region of the LIP phase space corresponding to forward walking, through

$$a(z_0)x_c(\theta^+(\alpha)) + b(z_0)d < L^+. \tag{25}$$

where $a = -\sqrt{gz_0}$, $b = \sin(\tan^{-1}(\sqrt{gz_0}))$, and $d > 0$. This constrains the post-impact x_c and L_y to lie at least a distance d further in the interior of the upper (walking) quadrant of the LIP phase space, and is used to replace (17) in (14).

D. Optimized Gait Design Process

The HZD optimization (14) – with (24) in place of (16) and (25) in place of (17) – can be used to generate stable, hybrid invariant walking gaits that also correspond to a local maximum in energy efficiency. The process of designing a gait through this method consists of configuring the initial condition and the specific values of the constraints. The next section presents experimental results from implementation of a gait produced by this and the implicit gait design processes.

V. Experimental Implementation on AMBER-3M

This section presents results from implementation of the two mechanics-based gait design strategies, discussed in Sections III and IV, that produce parameterized functions and corresponding fixed points encoding the respective gaits; inverse kinematics on these functions and joint-level position control is used to experimentally realize the gaits.

A. AMBER-3M

The experiments in this research were performed on AMBER-3M, a planar bipedal robot developed at the Georgia Institute of Technology. AMBER-3M's total mass and leg length are 21.56kg and 0.873m, respectively, and the height of AMBER-3M's center of mass when standing with straight legs is 0.896m. A key component of the mechanical design that enabled this work is its *modularity*: AMBER-3M was designed with modular segments, such as calves and thighs, for the purpose of testing out a wide variety of behaviors. In this study, a pair of underactuated legs – each with a rounded bottom – are attached to the robot, resulting in a single point of contact with the ground. This robot-ground contact interface is necessary to achieve the underactuated angular momentum mechanics discussed in Section II-B. The robot is connected to the world through a 3.35m radius circular boom which eliminates motion in the lateral direction.

The control structure of AMBER-3M is implemented on two levels, high and low level control. The high level controller is dominated by a onboard cRIO from National Instrument, running LabVIEW2015 with control frequency 200Hz. At this level, the actual measured joint positions and velocities are used to calculate desired positions and velocities via inverse kinematics on the functions produced by the gait design methods; these desired positions are then converted into desired torques via PD control, see [17] for more details. On the low level, ELMO motion controllers collect encoder data and perform current/torque control.

B. Implicit MBC Gait Design

The first experimental gait was designed via the method described in Section III, which generates a gait by simulating the closed-loop hybrid walking model under the action of the mechanics-based controller. The following describes the specific choice of MBC parameters and the rationale behind each choice: $x_c^* = -0.12\text{m}$ provides a relatively "conservative" stride length, $L_y^* = 0.6$ provides a conservative forward walking speed for the choice of x_c^*, $z_n^{max} = 0.08\text{m}$ results in large foot clearance, $z_0 = 0.87\text{m}$ results in a "high" nominal center of mass height and reduces knee flexion and $\delta_z = 0.03\text{m}$ results in lower joint velocities than other values of δ_z for a fixed choice of the previous parameters.

C. Optimized Gait Design

The second experimental gait was designed via the method described in Section IV. For this work, we employed a collocation based optimization algorithm, based on [12], to solve the nonlinear programming problem (14) with the mechanics-based HZD stability constraint (24) and forward walking constraint (25). In particular, due to the complex nonlinearity of the robot dynamics and constraints, we employed a *pseudospectral method* [8] to boost the efficiency and robustness of optimization process. Additional boosts in efficiency are gained by pre-computing the analytical Jacobian of each constraint with the use of *defect variables*. The resulting nonlinear program is solved after 84 iterations and 0.54 seconds with a constraint violation $6e^{-11}$ via IPOPT [1] using the linear solver ma57.

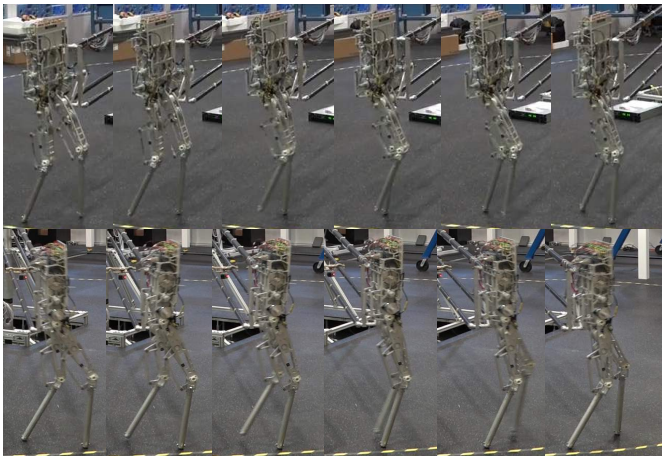

Fig. 3. Snapshots from experimental implementation of the two gait design methods on AMBER-3M. (Top) An Implicit Mechanics-Based gait produced by the methods described in Section III. (Bottom) An optimized gait with mechanics-based constraints produced by the method in Section IV.

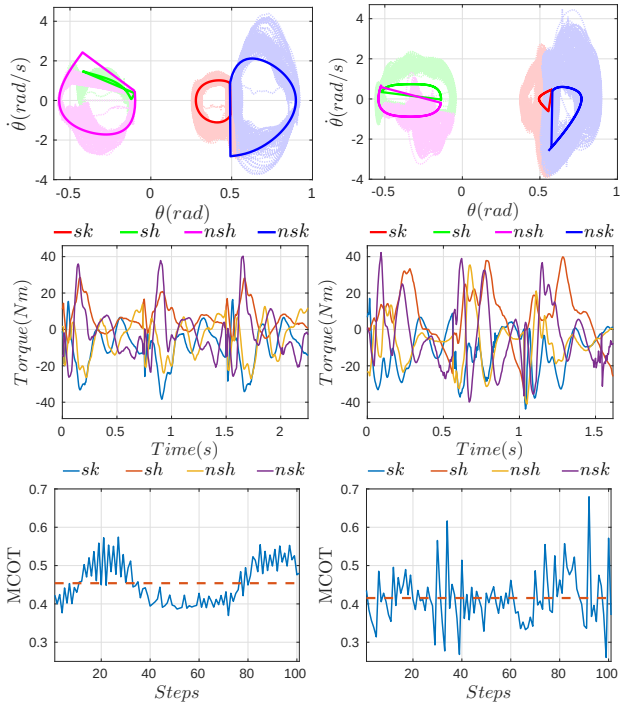

Fig. 4. Experimental results from implementation of the gait design strategies. (Left Column) Implicit MBC gait experiments. (Right Column) Optimized gait experiments. (Top row) Experimental and simulated phase portraits. (Middle row) Experimental torques for selected steps. (Bottom row) Mechanical cost of transport over several steps in each experiment.

D. Experiment Method and Results

Results from experiments with the implicit MBC gait are shown in the left column of Fig 4 and similarly, the optimized gait experiment results are shown in the right column of Fig 4. Note that the observed joint velocities in experiments, shown in the phase portraits in the top row, are much higher than the velocities in the simulated gaits. The leading hypothesis for this discrepancy is that the slope of the lab floor varies around the circular walking path, and as both gaits are designed for flat ground, the robot tends to gain and lose speed on different parts of the track. Joint torques from selected steps in experiment are shown in the middle row of Fig. 4 and the mechanical cost of transport is shown in the bottom row; this is calculated via

$$MCOT_i = \frac{1}{Mgd_i} \int_0^{T_i} \sum_j |\dot{\theta}_j(t) u_j(t)| dt \qquad (26)$$

where d_i and T_i are the distance traveled and duration of the i^{th} step. Snapshots from the experiments are shown in Fig. 3, and a movie of the experiments is available online [2].

The two methods produced noticeably different walking behaviors: the implicit MBC gait exhibits less torso movement, but larger knee flexion and higher swing foot height than the optimized gait. These discrepancies are expected as the nonlinear program used to obtain the optimized gait is largely a "black box". Locally optimal solutions of this nonlinear program often correspond to gaits with non-intuitive characteristics. The intent of this paper is to demonstrate that both methods are capable of producing gaits which can be successfully implemented experimentally, as shown in these *initial results*. An extensive study comparing the merits of the two methods is an objective of future work.

VI. Conclusion and Future Work

This paper presents the first experimental realization of gaits designed using the mechanics-based principles proposed in [20]. While the robot successfully completed several laps around the lab with the two gaits considered, the experimental implementation can be improved in a number of ways. One goal of future work is to improve estimation of the angular momentum about the stance pivot so that the full mechanics-based controller with angular momentum feedback can be employed on the hardware. Another action item is to improve the efficiency of the implementation and attempt to reach specific cost of transport numbers closer to those reported in other underactuated walking implementations, such as [5]. The ultimate goal is to use lessons learned from planar experiments to guide the mechanics-based design of 3D humanoid gaits.

References

[1] `https://projects.coin-or.org/ipopt`.

[2] `https://youtu.be/xw8jaDz8XTc`.

[3] A. D. Ames. Human-inspired control of bipedal walking robots. *IEEE Transactions on Automatic Control*, 59(5):1115–1130, 2014.

[4] C. Chevallereau, J. W. Grizzle, and C. H. Moog. Nonlinear control of mechanical systems with one degree of underactuation. In *IEEE International Conference on Robotics and Automation (ICRA)*, pages 2222–2228, 2004.

[5] E. Cousineau and A. D. Ames. Realizing underactuated bipedal walking with torque controllers via the ideal model resolved motion method. In *IEEE International Conference on Robotics and Automation (ICRA)*, pages 5747–5753, 2015.

[6] X. Da, O. Harib, R. Hartley, B. Griffin, and J. Grizzle. From 2D design of underactuated bipedal gaits to 3D implementation: Walking with speed tracking. *IEEE Access*, 4:3469–3478, 2016.

[7] H. Goldstein, C. Poole, and J. Safko. *Classical Mechanics*. Addison Wesley, 2002.

[8] D. Gottlieb and S. Orszag. *Numerical Analysis of Spectral Methods*. Society for Industrial and Applied Mathematics, 1977.

[9] B. Griffin and J. Grizzle. Nonholonomic virtual constraints for dynamic walking. In *IEEE Conference on Decision and Control (CDC)*, pages 4053–4060, 2015.

[10] J. W. Grizzle, C. Chevallereau, R. W. Sinnet, and A. D. Ames. Models, feedback control, and open problems of 3D bipedal robotic walking. *Automatica*, 50(8):1955 – 1988, 2014.

[11] J. W. Grizzle, F. Plestan, and G. Abba. Poincaré's method for systems with impulse effects: application to mechanical biped locomotion. In *IEEE Conference on Decision and Control (CDC)*, pages 3869–3876, 1999.

[12] A. Hereid, S. Kolathaya, and A. D. Ames. Online hybrid zero dynamics optimal gait generation using legendre pseudospectral optimization. In *to appear in IEEE Conference on Decision and Control*, 2016.

[13] C. Hubicki et al. ATRIAS: Design and validation of a tether-free 3D-capable spring-mass bipedal robot. *The International Journal of Robotics Research*, 2016.

[14] M. Johnson et al. Team IHMC's lessons learned from the DARPA robotics challenge trials. *Journal of Field Robotics*, 32(2):192–208, 2015.

[15] S. Kajita and K. Tani. Study of dynamic biped locomotion on rugged terrain-derivation and application of the linear inverted pendulum mode. In *IEEE International Conference on Robotics and Automation (ICRA)*, pages 1405–1411, 1991.

[16] D. Kim, G. Thomas, and L. Sentis. Continuous cyclic stepping on 3D point-foot biped robots via constant time to velocity reversal. In *International Conference on Control Automation Robotics Vision (ICARCV)*, pages 1637–1643, 2014.

[17] W. L. Ma, H. H. Zhao, S. Kolathaya, and A. D. Ames. Human-inspired walking via unified PD and impedance control. In *IEEE International Conference on Robotics and Automation (ICRA)*, pages 5088–5094, 2014.

[18] B. Morris and J. Grizzle. A restricted poincaré; map for determining exponentially stable periodic orbits in systems with impulse effects: Application to bipedal robots. In *IEEE Conference on Decision and Control (CDC)*, pages 4199–4206, 2005.

[19] H. W. Park, S. Park, and S. Kim. Variable-speed quadrupedal bounding using impulse planning: Untethered high-speed 3D running of MIT cheetah 2. In *IEEE International Conference on Robotics and Automation (ICRA)*, pages 5163–5170, 2015.

[20] M. J. Powell and A. D. Ames. Mechanics-based control of underactuated 3D robotic walking: Dynamic gait generation under torque constraints. In *to appear in IEEE International Conference on Intelligent Robots and Systems (IROS) 2016*.

[21] J. Pratt, J. Carff, and S. Drakunov. Capture point: A step toward humanoid push recovery. In *IEEE International Conference on Humanoid Robots*, pages 200–207, 2006.

[22] H. Razavi, X. Da, and A. Bloch. Symmetric virtual constraints for periodic walking of legged robots. In *to appear in IEEE Decision and Control (CDC)*, 2016.

[23] J. Reher, E. A. Cousineau, A. Hereid, C. M. Hubicki, and A. D. Ames. Realizing dynamic and efficient bipedal locomotion on the humanoid robot DURUS. In *IEEE International Conference on Robotics and Automation (ICRA)*, pages 1794–1801, 2016.

[24] S. S. Sastry. *Nonlinear Systems: Analysis, Stability and Control*. Springer, New York, 1999.

[25] B. Stephens and C. Atkeson. Push recovery by stepping for humanoid robots with force controlled joints. In *IEEE International Conference on Humanoid Robots*, pages 52–59, 2010.

[26] M. Vukobratović and B. Borovac. Zero-moment point–thirty-five years of its life. *International Journal of Humanoid Robotics*, 01(01):157–173, 2005.

[27] E. R. Westervelt, J. W. Grizzle, and D. E. Koditschek. Hybrid zero dynamics of planar biped walkers. *IEEE Transactions on Automatic Control (TAC)*, 48(1):42–56, 2003.